16

Molecular Desorption by Laser–Driven Acoustic Waves: Analytical Applications and Physical Mechanisms

Alexander Zinovev, Igor Veryovkin and Michael Pellin
Argonne National Laboratory
USA

1. Introduction

Analytical mass-spectrometry (MS) is a powerful, widely-used tool for materials analysis, helping to make progress in materials and environmental sciences, chemistry, biology, astrophysics, etc (Dass 2007). Often the sample to be studied (analyte) is a solid requiring: a) volatilization/desorption of the analyte atoms/molecules and b) their consequent conversion to the charged particles (ionization) prior to mass analysis. The last two decades have seen revolutionary advances in these techniques (Dass 2007) and the use of direct laser irradiation to achieve volatilization is one of the wide-spread methods (Lubman 1990) These pulsed laser-based techniques for the desorption/emission of the atoms, molecules and ions from the surface of solids has benefitted from fundamental study of the process beginning with the invention of the lasers (Honig and Woolston 1963) . A short laser pulse hitting a solid absorbing surface delivers high energy in a small volume inducing a variety of state changes. One consequence is the evaporation/desorption of surface atoms and molecules could be used for further analysis by MS technique. However, the increasing use of MS methods in analytical chemistry of organic and biomolecules revealed that this direct desorption process had significant drawbacks for the analysis of molecular solids. Most importantly, the high energy density produced during irradiation results in not only surface heating but also in excitation of internal vibrational and electronic states of desorbed molecules leading to their partial or even complete fragmentation (Lubman 1990). This difficulty was overcome for many samples by the development of Matrix Assisted Laser Desorption and Ionization (MALDI), which by imbedding the analyte in a specialized UV absorbing molecular solid (the "matrix") allows UV lasers to both desorb and ionize large organic and biomolecules without significant fragmentation (Cole 2010). Because MALDI combines both of the needed initial processes (desorption and ionization) it very quickly following the pioneering publication (Karas, Bachmann et al. 1985) became a key analytical tool. MALDI is now one of principle research tools in proteomics (Cole 2010) and its discovery was recognized with the Nobel Prize in chemistry in 2002.

Despite the success of the MALDI technique current active areas of research include quantification and analysis in the low mass region. Application of MALDI to analyte quantification while possible requires careful attention to matrix/analyte sample

preparation, a detailed understanding of the crystallization process with regard to the analyte, and careful many spot analyses (to find the sample signal average which often varies by orders of magnitude as a function of laser position). (Duncan, Roder et al. 2011)

This desire to find a discriminative, sensitive and more easily quantifiable alternative to MALDI has lead us to re-examine another molecular desorption method that doesn't require the use of a matrix. The first observation of this method of molecular desorption (later called Laser Induced Acoustic Desorption, LIAD) belongs (to the best of our knowledge) to B. Lindner (Lindner and Seydel 1985). This observation has been followed by several studies including (Golovlev, Allman et al. 1997) where the abbreviation LIAD was introduced and by (Perez, Ramirez-Arizmendi et al. 2000) who applied the technique to several classes of MS problems.

LIAD has rather simple experimental layout: an analyte is deposited onto the front surface of thin metal foil (the substrate), which is irradiated from the back (i.e. the side opposite to both the analyte and the mass spectrometer) by a pulsed laser beam with power density insufficient to pierce the foil. Such irradiation results in the volatilization of the analyte. The volatilization is largely in the form of neutral molecules that can be utilized for further MS analysis using an appropriate post-ionization method. The method seems to be relatively insensitive to the sample preparation method. Commonly the sample preparation requires only evaporating a drop containing a few nano-moles of the analyte. Remarkably little desorption induced fragmentation is seen when a suitable "soft" ionization method such as VUV photoionization can be found. It is also useful to note that while the molecular signal depends on drive laser intensity the fragmentation observed varies only weakly.

The advantages of LIAD have been demonstrated by many researchers; however, the mechanism is not well understood. The first desorption mechanism was proposed (Golovlev, Allman et al. 1997). It was supposed that because the metal is opaque and completely blocks the direct interaction between the drive laser light and adsorbed, front-side molecules, the only possible way of energy transfer is the mechanical. In this model, the interaction of laser pulse with metal foil backside resulted in formation of acoustic waves that move through the foil inducing a front surface oscillation motion. The molecules that are sitting on this surface desorb due to a simple "shake-off" mechanism similar to those that we use to remove dust particles from our clothes by shaking it.

A difficulty with this model arises when considering the relatively strong surface binding energy experienced even by physisorbed molecules. In order to be efficiently desorbed from the surface, surface molecules need to achieve initial kinetic energies exceeding their surface binding energies (typically in the range of 0.05 - 0.5 eV for physically adsorbed molecules (Adamson and Gast 1997)). This corresponds to velocities of a few hundred m/s for molecules with masses of a few hundred atomic mass units. Unfortunately, acoustic vibrations have mass transfer velocities much lower than the speed of sound, and in elastic deformation mode, this velocity does not exceed a few m/s (Landau and Lifshits 1987). While laser-driven acoustic wave generation in metals is very well studied problem (Hutchins 1985), the physics of their generation in metal foils is crucial to understanding the need for development of new desorption mechanisms. In the next paragraphs we will give a brief theoretical overview and will present our experimental results on laser-driven acoustic waves in thin metal foils.

2. Laser-driven acoustic waves in thin metal foils

The interaction of pulse laser beam with metal surface is very complex phenomenon but our specific interest is in formation of the acoustic waves in irradiated material. To generate an acoustic wave a time dependent stress needs to be applied to the solid. A laser pulse is an excellent tool to generate this kind of the stress. There are two principal mechanisms of laser-induced stress formation in the solids: a) thermal stress, resulted from the non-uniform heating of the irradiated surface by the laser beam; b) mechanical stress due to mechanical impulse transferred from the leaving plasma plume formed on the surface during laser ablation. The parameters of the acoustic waves generated for these two processes are slightly different and will be discussed in details later. Here we will use acoustic wave theory but one should note that its' use is applicable only when the magnitude of the applied stress is small in comparison with the Young's modulus of the material. Large applied stresses can cause the development of the shock waves a phenomenon with different characteristics than acoustic waves (Menikoff 2007). Shock waves have been also hypothesized to be the driver of the LIAD phenomenon, and, as such cannot be entirely excluded from consideration, especially in some extreme cases. Nevertheless, during the last decade, laser-driven acoustic waves emerged in the literature as the "prime suspect" in the LIAD case.

2.1 Acoustic waves in metal foils

The general governing equation for the generation of elastic waves in solids can be derived by combining the equation of motion and the Hooke's law. In general case it is a differential tensor equation, which interconnects the stress tensor, applied to the body, the displacement of the body's elemental volumes (strain), and their elastic properties. In order to analyze the data in detail, the appropriate stress tensor needs to be determined, and the corresponding set of partial differential equations for strain and stress must be resolved (Pollard 1977). One can simplify this analysis by taking into account specifics of the experiments. For thin foils with $h/R_0<<1$ (where R_0 is the radius of the target foil, and h is its thickness), a round thin plate approximation can be applied to describe and analyze this problem (Smith 2000). The rise of the strain due to laser heating and the consequent development of the plasma plume can be considered as an external driving force. Generally speaking, the thin plate equation is a differential equation of the forth order,

$$\left(\frac{\partial^2}{\partial r^2}+\frac{1}{r}\cdot\frac{\partial}{\partial r}+\frac{1}{r^2}\cdot\frac{\partial^2}{\partial\theta^2}\right)^2\xi+v_L^{-2}\cdot\left(2\cdot\alpha\frac{\partial\xi}{\partial t}-\frac{\partial^2\xi}{\partial t^2}\right)=F(r,t) \tag{1}$$

where $\xi=\xi(r,t)$ is the surface displacement in the z direction (perpendicular to the sample surface), $F(r,t)$ is the external driving force caused by the laser irradiation, v_L is a parameter depending on the material density, ρ, thickness, h, and flexural rigidity, D. Furthermore,

$$v_L=\sqrt{D/\rho\cdot h}\ \text{, and }\ D=(N\cdot h^3/12\cdot(1-\varepsilon^2)) \tag{2}$$

where ε is the Poisson ratio, N is Young's modulus and α is the oscillation decay constant. A vibrating thin plate is one of the most frequently analyzed mathematical problems, and its detailed analysis can be found elsewhere (McLachlan 1951; Smith 2000). In the discussion given below, we will remain in the framework of the analysis given by (Smith 2000).

Assuming separate solutions for the radial and tangential terms, Eq. (1) can be converted into a system of three differential equations of the second order. Being primarily interested in the foil displacement in normal (z) direction to the surface at the epicenter (r=0) and assuming that the external driving force $F(t)$ is a pulse function lasting a specific time τ, we can separate the variables in the Eq. (2) for $t>>\tau$. Under the assumption of harmonic motion for all modes, the surface displacement can be expressed as $\xi(r,t)=\xi_1(r)\cdot e^{i\omega_{m,n}t-\alpha\cdot t}$, where $\omega_{m,n}$ is the vibration frequency. The general governing equation can then be written in the following form:

$$\left(\frac{\partial^2}{\partial r^2}+\frac{1}{r}\cdot\frac{\partial}{\partial r}-\frac{n^2}{r^2}\pm k_{n,m}^2\right)\xi_1=0 \tag{3}$$

where n is an integer number, $k_{n,m}=\omega_{n,m}/v_L$ and v_L is the wave velocity as in Eq.(2).
Under the assumption that the oscillations are harmonic and decay exponentially, the following solution for the surface displacement can be obtained (McLachlan 1951):

$$\xi_n(r,t)=\xi_0\cdot\left(J_n(k_{n,m}r)+\chi\cdot I_n(k_{n,m}r)\right)\cdot\exp(i\omega_n t)\cdot\exp(-\alpha\cdot t) \tag{4}$$

where J_n and I_n are Bessel functions and χ is a constant. The term describing the angular dependence of the oscillations is omitted in Eq.(4). The fact that foils used in LIAD experiments are typically glued or welded on their perimeter corresponds in our analysis to the situation when edges of the round plate are fixed (i.e. non-vibrating), and is described by the following boundary conditions:

$$\xi(R_0,t)=0,\frac{d\xi(R_0,t)}{dt}=0\ , \tag{5}$$

that lead to an equation, whose solutions $j_{n,m}$ have tabulated values (Smith 2000). The corresponding vibration frequencies, $\omega_{n,m}$, can be then expressed as

$$\omega_{n,m}=\sqrt{j_{n,m}^4\cdot\frac{v_L^2}{R_0^4}-\alpha^2}\approx\frac{j_{n,m}^2\cdot h}{R_0^2}\cdot\sqrt{\frac{N}{12\rho\cdot(1-\varepsilon^2)}} \tag{6}$$

Because values of α are small compared to the first term under the square root sign in Eq.(6), it is a reasonable assumption that the frequency is proportional to the square root of the ratio of Young's modulus, N, to the density of the foil material, ρ. As described by Eq. (6), in the steady-state regime (driving force $F(t)$=0 for $t>>\tau$) the frequency spectra and decay times of the oscillation will remain the same while the laser intensity is varied, and only the amplitude should change.
For short times, ($t<\tau$), the approach to solving Eq.(1) is to assume that the external force is a delta-function in space $F(r,t)=F(t)\delta(r)$ (point source), allowing the solution of Eq.1 to be expressed in the form

$$\xi(r,t)=g(r)\cdot\xi(t) \tag{7}$$

where $g(r)$ and $\xi(t)$ represent the spatial and the time dependencies of the final solution, respectively. This approximation should help to develop a clearer understanding of physical problems related to the laser generation of acoustic waves in thin foils.

Using Eq. (7), Eq. (1) can be split into two independent equations, with the equation for $\xi(t)$ having the form

$$\frac{d^2\xi}{dt^2} - 2\cdot\alpha\cdot\frac{d\xi}{dt} + \omega_n^2\cdot\xi = F(t)\,, \tag{8}$$

and the equation for $g(r)$ being a non-uniform Bessel equation with the $\delta(r)$- function in the right side of it.
The exact solution of Eq. (8) can be expressed as the convolution of the Green function of the problem (8) and real time shape of $F(t)$. The governing equation for the Green function will be Eq.(8) with δ-function in the right side. It can be easily derived by applying the Laplace transform to the Eq.(8), subsequently solving the obtained linear equation in the s-space and returning back to the time space with using the inverse Laplace transform. As a result of these procedures, one can finally obtain the following equation

$$\xi_n(t) = \int_o^t \frac{e^{-\alpha\cdot(t-\tau)}}{\sqrt{\omega_n^2-\alpha^2}}\cdot\sin\left[\sqrt{\omega_n^2-\alpha^2}\cdot(t-\tau)\right]\cdot F(\tau)d\tau\,, \tag{9}$$

and the complete solution of Eq.(8) can then be obtained as the sum of the components of Eq.(9) over n.
Thus, the generation of acoustic waves in thin foils can be described by Eq.(9) which strongly depends on driving force $F(t)$ after whose cease the vibration evolves into decaying harmonic oscillations (Eq.(4)) with frequencies defined by Eq.(6). It is apparent that maximal surface velocities can be achieved only at the initial stage of acoustic wave generation when $t<\tau$. The application of Eq.(9) to analysis of laser-driven acoustic vibrations is complicated by the lack of the exact knowledge of the time profile of the driving force $F(t)$. Depending on regime of the surface irradiation, this force may be of different origins and, accordingly, have strongly varying magnitudes and time profiles. The appropriate mechanisms will be discussed in the following section.

2.2 Generation of the acoustic waves by laser pulses

2.2.1 The action of laser pulse on the metal surface: heating and plasma generation

Metals subjected to pulsed laser irradiation absorb energy within a very thin surface layer (the skin-depth for most metals is less than 10^{-7} m) so that the temperature of the irradiated surface can rise extremely fast. For moderate laser intensities (below the plasma formation threshold) and a Gaussian-shaped laser beam, the maximum surface temperature can be estimated using a well-known expression (Prokhorov, Konov et al. 1990)

$$T_{\max}(0) = 2.15\frac{AI_{\max}\tau^{1/2}}{(\pi c\rho \mathrm{K})^{1/2}}\,, \tag{10}$$

where $T_{max}(0)$ is the maximum surface temperature at z=0 (z direction is orthogonal to the target surface), A is the laser radiation absorption coefficient, I_{max} is the peak laser power, τ is the laser pulse duration, and c, ρ, and K are the specific heat, density and thermal conductivity of the corresponding metal, respectively.
After cessation of the laser pulse, the adsorbed energy continues to diffuse into the bulk metal and along the metal surface, resulting in a temperature increase underneath the

irradiated spot and outward from the spot along the surface. Temperature evolution at any moment, $t>\tau$, and for any position, $z>0$, proceeds according to the following equation (Prokhorov, Konov et al. 1990):

$$T(z,t)=\frac{2AI_{\max}\gamma^{1/2}}{\mathrm{K}}\cdot[t^{1/2}ierfc(\frac{z}{2(\gamma t)^{1/2}})-(t-\tau)^{1/2}\cdot ierfc(\frac{z}{2[\gamma(t-\tau)]^{1/2}})] \tag{11}$$

where γ is the thermal diffusivity of the metal, which can be expressed as $\gamma=\mathrm{K}/c\rho$.
The function $ierfc(x)$ is given by

$$ierfc(x)=\pi^{-1/2}\{\exp(-x^2)-x(1-erf(x))\} \tag{12}$$

where $erf(x)=\frac{2}{\sqrt{\pi}}\int_0^x\exp(-\xi^2)d\xi$

Eqs. (10) and (11) are the solutions of the one-dimensional heat diffusion equation and are valid only if the laser beam size, r_0, is significantly greater than both the foil thickness h and the thermal diffusion length l_{th} calculated as $l_{th}=(\gamma\cdot t)^{1/2}$.
The strong rise of the surface temperature given by Eq.(10) results in the surface melting and evaporation, as well as in plasma plume formation (ablation regime) (Miller and Haglund 1998). Despite the fact that laser plasma generation and evolution have been the focus of numerous studies, no general mechanisms exist that describe the plasma recoil pressure on the surface for a broad range of laser intensities (Phipps, Turner et al. 1988), due to the complexity of the phenomenon. For GW/cm² peak laser powers, hot and dense plasma is formed in the vicinity of the surface, which can screen the surface and prevent laser radiation from reaching it. In this case, the ablative pressure very weakly depends on the target material parameters (Phipps, Turner et al. 1988) and has a sub-linear dependence on laser intensity. In a semi-regulating, one-dimensional plasma model (which can be applied to our case as a simplified, first-order approximation), this equation is written, as follows (Gospodyn, Sardarli et al. 2002) :

$$P_{a,\max}\approx 7.26\cdot 10^8\cdot I^{3/4}\cdot(\lambda\cdot\sqrt{\tau})^{-1/4}\,, \tag{13}$$

where I is expressed in GW/cm², λ in microns, τ in nanoseconds and $P_{a,max}$ in Pa. While Eq. (13) was derived for an aluminum target in vacuum and for a supercritical plasma density, it exhibits only a weak dependence on the atomic mass, A, of the material irradiated ($A^{-1/8}$) (Gospodyn, Sardarli et al. 2002) and may be applicable to specific experiments only as an upper limit estimate. For lower laser intensities (<1 GW/cm²), the plasma plume transmittance strongly varies with laser intensity (Song and Xu 1997), depending upon the plasma density and temperature. In this case the evaporated surface material is ionized only partially and the total mass of the evaporated atomic cloud are exponentially increasing with the surface temperature and, hence with the laser intensity (Murray and Wagner 1999).

2.2.2 Thermal and plasma driven acoustic waves in metal foils

The temperature rise, as heat is transported into the solid causes linear thermal expansion resulting in the development of thermoelastic acoustic waves in the irradiated metal. Eqs. (10) and (11) can be used to determine the driving force which produces the waves. In

accordance with the general theory of thermal stresses in thin plates (Boley and Weiner 1960), a non-uniform heating of the surface is equivalent to a *negative loading pressure* and may be expressed as

$$P_T = -\frac{N \cdot \eta}{1-\varepsilon} \cdot \nabla_r^2 \left[\int_{-h/2}^{h/2} T(r,z) \cdot z dz \right], \tag{14}$$

where the temperature distribution over z is described by the Eq. (11) and η is the linear thermal expansion coefficient.
If the loading force is negative (i.e., directed backwards, towards the heating laser beam, Eq. 14), it is not surprising that an initial depression observed in the foil surface is opposite to the heating laser beam. Similar results have been reported in the literature (Scruby 1987) for thicker metal samples where the thin plate approximation was not applicable. Maximum amplitudes and shapes of the observed depression vary for different metals and are defined by both the temperature profile (Eq. (11)) and by elastic properties of the material.
In the case of plasma formation, the situation becomes more complex. The amplitude of the driving force can be estimated using an expression similar to Eq.(13), whereas the time profile of generated stress pulse is the subject of experimental study (Krehl, Schwirzke et al. 1975). Laser plasmas formation and their interaction with the surface is very complex and multi-variable problem, which can only be solved in the framework of some model assumption (Mora 1982). This is why direct experimental studies of laser-driven surface vibrations should be an essential part of any acoustic wave related desorption phenomena.

2.2.3 Experimental observations of laser-generated acoustic waves in thin foils

Experimental studies of acoustic waves in solids due to pulsed laser irradiation have started with the advent of such lasers (White 1963). A great collection of experimental results and theoretical analyses of acoustic wave generation in solids driven by laser pulses has been accumulated since (Hutchins 1985), and these studies continue at present (Xu, Feng et al. 2008). Regrettably, there is a very limited data set, which could be used to interpret of LIAD experiments. To prove (or disapprove) the "shake-off" hypothesis of molecular desorption, direct measurements of thin foil surface velocities in back-side irradiation geometry are required. The scarcity of such data motivated us to setup a series of our own experiments aiming at measurements of thin foils vibrations under typical LIAD conditions. Experimental approaches to this problem are well known and described in the literature (Scruby and Wadley 1978; Royer and Dieulesaint 2000). Nevertheless, we will briefly describe below our system, in order to create a better stage for presentation and discussion of the original results.

2.2.3.1 Experimental technique: optical and electrical methods

One of the most popular and widely used methods to studies of acoustic waves is based on non-contact optical measurements. Figure 1a shows the experimental setup for measurements of surface displacement using interferometry-based approach. A He-Ne laser (1) (Melles-Griot, 543 nm, 0.5 mW) was used as the light source for a Michelson interferometer. It consisted of a beam splitter (5), an etalon and steering mirrors (3, 4), a focusing lens (6), a target (7), an imaging lens (9), an aperture (13), a focusing lens (14) and a photomultiplier (15). The target was back-irradiated by a pulsed laser (12) through a fused silica lens (8). Laser beam parameters were measured by intersecting the laser flux with two

partially reflecting (8%) quartz plates (10, 11) directing reflected beams onto a fast photodiode (16) and an energy meter (17), respectively. A wedge-type optical attenuator (18) was used to balance the Michelson interferometer shoulders and to increase the contrast of the resulting interference pattern. Focusing lenses (6) and (8) were mounted on three-axis translation stages. In this arrangement, both the acoustic-wave generating and diagnostic laser beams could be independently focused and translated to different points on the target surface. A lens (9) formed the magnified interference pattern in the plane of an aperture (13) whose diameter was selected to be equal to the width of the dark band of the lowest interference order. A second lens (14) was used to collect the light, which passed through the aperture (13), and to direct it to the photomultiplier (PMT, 15).
The anode of the PMT was terminated with a 50 Ohm load to allow optical signals with rise times as short as 5 ns to be measured. This capability was confirmed by demonstrating that the shape of a 12 ns, NdYAG laser pulse was identical when measured by using this detection system and by a high-speed avalanche photodiode. The measurements bandwidth was limited by the PicoScope 3206 oscilloscope (200 MHz bandwidth and 200 Ms/s sampling rate), which was used for signal acquisition. The digitized PMT signal was transmitted to a PC via USB port and stored for further processing. The oscilloscope was triggered by a pulse from the fast photodiode (17). The measured lag between the trigger signal and the PMT signal was less than 40 ns. The maximum signal amplitude, corresponding to the peak-to-valley ratio of the interference pattern, was 80 mV. The minimum detectable signal was 5 mV at signal-to-noise ratio of about 3, which corresponds to a surface displacement of approximately 25 nm. However, because of the strong electrical noise generated by the Q-switch of the laser, the smallest surface displacement detectable in this series of experiments was about 40 nm.

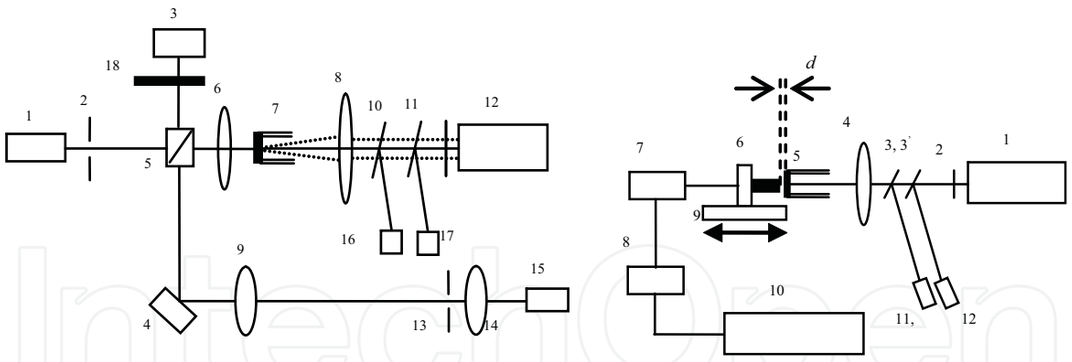

Fig. 1(a,b). Schematic drawing of the experimental setup for laser-driven acoustic wave studies. (a) Interferometry method; (b) Capacitance method

The same target irradiation scheme as described above was also used for the capacitance transducer measurements (Fig.1b). In contrast to the previous approach, a metal pin was placed in front of the target. This pin served as the second plate of a capacitor whose first plate was the target. These two capacitor electrodes were separated by a small gap *d*, typically about 100 μm. Both the target and the pin were fixed in optical mounts that allowed alignment in the plane of the sample surface. In addition, the mount of the pin was placed on a translation stage (9), driven by a picomotor, which could move the target (with the precision of 1 μm) in the direction orthogonal to the target surface. The pin had a diameter of 3 mm and its end was polished flat. In general, the design of this detector is

similar to that described in Ref.19. The pin was connected to the input of a miniature charge amplifier (7) powered by a constant (20 mA) direct current (DC) supply (8) and connected to the oscilloscope (10). The bandwidth of the charge amplifier was about 2 MHz, which provided a signal rise time of less than 400 ns. To increase the overall sensitivity of the detector, a positive bias potential of 100 V was applied to the target.
The sensitivity of the transducer to surface displacement can easily be expressed in terms of a planar capacitor

$$\Delta q = \frac{-\varepsilon VS}{d^2}\Delta d \tag{15}$$

where Δq is the change in the electric charge, V is the applied voltage, S is the surface area of the pin tip, d is the width of the gap between the electrodes and Δd is the change of the width. The sensitivity of the charge preamplifier was 10 mV/pC, which corresponded to a minimal detectable signal of about 5 mV (thus yielding reasonably good signal-to-noise ratio). With an applied bias potential of -100 V, the estimated detection limit of the transducer-based sensor was about 5 nm.

2.2.3.2 Experimental results: displacement and surface velocity of thin foils

Foils with various thicknesses (from 12.5 μm up to 100 μm) made from different materials were used in our experiments. Materials were selected to span the range from soft metals (Au, Al and Ni) to refractory metals (W, Mo and Ta) and semiconductors (Si). For each experiment, the front surface of the sample was mechanically polished to roughness of less than 0.250 μm (RMS). After polishing, the foils were glued with silver epoxy to the rim of a hollow quartz cylinder (8 mm outside diameter, 8 mm height, and 0.5 mm wall thickness). The epoxy was cured for 2 hours in an oven at temperature of 100° C. Due to the differences between thermal expansion coefficients of the foil materials and quartz, the foil stretched over the top of the quartz cylinder once the assembly cooled to room temperature. The tension was not very strong (according to our estimates, the total radial force did not exceed 1 N), and therefore, the foils in our experiments may be considered as supported at the edges. The silver epoxy also provided a conductive path between the sample and the instrument by placing a silver epoxy track along the quartz cylinder side.
Lasers generating both ultraviolet (UV) and infrared (IR) light were used for target irradiation. The UV light was generated by an ArF excimer laser (EX10-300, GAM, Inc.) having a wavelength 193 nm and a pulse duration of 15 ns. The output pulse energy could be varied from 0.4 to 4 mJ by using neutral density optical filters. The laser radiation was focused onto the backside of the target (opposite to the surface displacement sensors) using a fused silica lens with a focusing distance of f=300 mm. The irradiated spot on the target had rectangular dimensions of 100×500 μm, which corresponded to a UV laser power density in the range of 50–500 MW/cm². For IR irradiation of the target, a Q-switched Nd:YAG laser (Continuum) was used. This IR light had a wavelength of 1064 nm, a 12 ns pulse duration and an output energy in the range of 1–15 mJ/pulse. The IR laser beam had a Gaussian profile and produced a spot on the target surface with a nominal diameter of 500 μm, corresponding to peak power density of 40–600 MW/cm².
Waveforms representing foil oscillations were measured over the time range from 5 μs to 5 ms. For times much greater than the laser pulse duration ($t>>\tau$), a decaying quasi-harmonic oscillations were observed for all materials. The measured time dependence of the displacement of the foils irradiated by laser pulses with different intensities exhibited

qualitatively similar behavior, although amplitudes, frequencies and decay times varied. These results suggest that each foil behave as a mechanical system able to oscillate in a free-running mode after the external force is removed. Fast Fourier Transform (FFT) analysis applied to the measured data has shown that the frequency spectra consisted of discrete lines (modes) appearing in the range of 10–100 kHz.

In contrast to the steady-state regime ($t>>\tau$) when different foils oscillated very similarly, the initial moment ($t<\tau$) of the evolving oscillation was distinctly different for each foil. Fig. 2 presents the time dependence of the surface displacement for different metals at low irradiation intensities (50 MW/cm^2) for "early" times in the range up to 50 μs. For all measurements at low intensities, the initial displacement is found to be negative, indicating that the surface is first depressed (i.e. towards to the driving laser beam and, correspondingly, away from the detector). Increasing the laser intensity leads to the initial surface vibration waveform displacement changing from negative to positive. This is due to the recoil pulse which occurs when material is ablated from the irradiated surface due to plasma formation. Fig. 3 shows the time dependences of the displacement of Ta foil surface for different laser irradiation intensities. The plasma formation threshold for this Ta foil was ~220 MW/cm^2, as determined by the observation of the plasma plume glow in a separate experiment. The FFT analysis of the experimental data at higher laser intensities revealed that the frequency spectrum of the foil oscillations in the non-steady-state regime contains much higher frequency components than found for the steady-state case. After a few tens of microseconds, the high frequency components disappear as the foil oscillation become harmonic as described by Eq.(4).

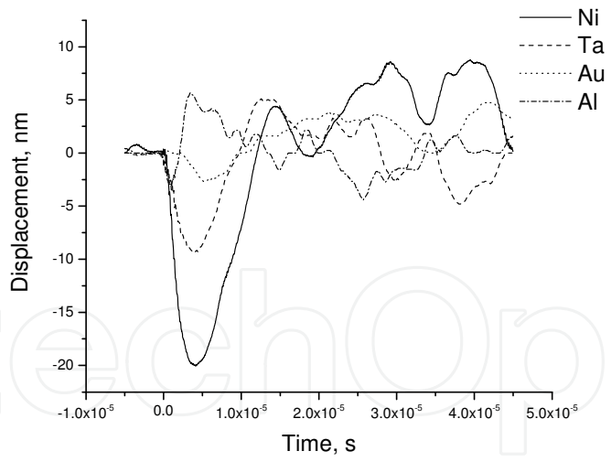

Fig. 2. Time dependent displacement for different metal foils at low laser intensities (50 MW/cm^2

The obtained results are in good agreement with time dependencies of surface displacement measured under slightly different experimental conditions (Hutchins 1985). This fact clearly demonstrates that laser-driven acoustic waves in thin metal foils have no experimental peculiarities distinguishing them from well-known acoustic wave mechanisms. This result allowed us to calculate surface velocities using the measured surface displacements (Fig. 4). As one can see from Fig.4, these velocities are indeed in the range of meters per second.

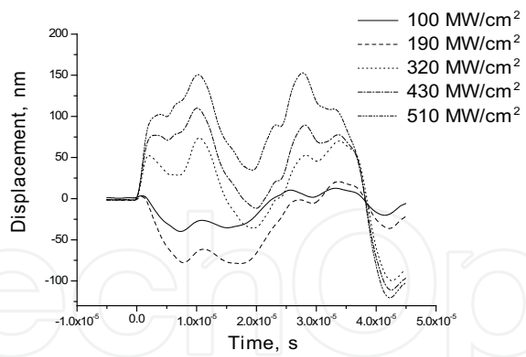

Fig. 3. Time dependent displacement of Ta foil (12.5 μm thick) at different laser intensities

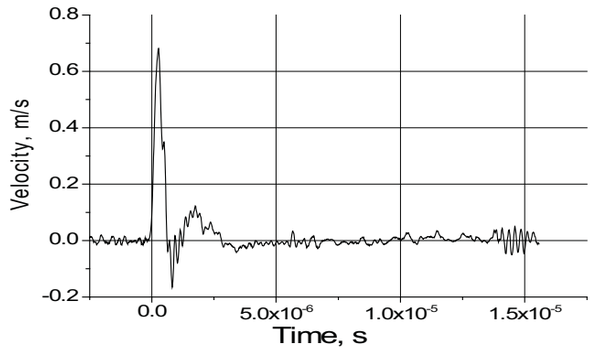

Fig. 4. Time dependence of Ta foil (12.5 mm thick) surface velocity at 400 MW/cm² driving laser intensity

This picture clearly confirms the statement above that the mass transfer velocity (or surface displacement velocity, in terms of our experiment) is much slower than the speed of sound in metals. In its turn, this result supports our hypothesis that the vibrational motion of the foil surface cannot serve as direct cause of molecular desorption, and that *the real physical mechanism of LIAD is not as simple as mechanical shake-off*.

3. Desorption of the molecules from back-irradiated thin metal foils

3.1 Laser desorption in modern MS: methods and applications

As shown in the previous sections, laser induced desorption phenomena play important role in modern MS. The primary role of the laser beam there is to deliver high energy density into some (typically small) volume of the analyte. Due to the local overheating this volume is volatilized forming hot and dense vapor plume, which might be partially ionized. This ionization phenomenon can be considered as a great advantage of laser desorption because there is no need for an additional ionization step, so that the desorbed ions may be directly analyzed by a mass-spectrometer. At the same time, this can be a significant drawback, because, due to collisions in the plume, organic molecules may fragment to the point that their mass analysis becomes meaningless (Miller and Haglund 1998). While using UV lasers in MS analyses of organic materials often produced encouraging results, it is well recognized in the literature that "general mechanism that is applicable to all organic solids

at all UV wavelengths does not exist"(Srinivasan and Braren 1989). The introduction of MALDI gave strong indication that many problems, associated with laser desorption MS might have been solved. However despite popularity of MALDI in MS analyses of proteins, lipids and many other organics (Schiller, Suss et al. 2007), this method cannot be considered as universal because it requires to identify efficient matrix substances for different organic species, and often to develop specialized sample preparation protocols. And, regrettably, MALDI MS cannot be used to directly characterize mixtures of unknown molecules. This is why the search for more versatile and universal methods of molecular desorption/ionization is still on in the analytical mass spectrometry community. From this perspective, the ability of LIAD to volatilize different kinds of organic molecules without noticeable (or, very often, without any) fragmentation has attracted strong interest among researchers.

3.2 Laser-induced acoustic desorption

As described above, the acronym LIAD was suggested in the work conducted by the Chen's team (Golovlev, Allman et al. 1997) where the hypothesis about the acoustic wave nature of the desorption process was expressed. However, LIAD remained just an interesting observation until Kentamaa's team of researchers from Purdue University (Perez, Ramirez-Arizmendi et al. 2000) took on it and demonstrated successful applications of LIAD for the MS analysis of different organic species like cytosine, guanine, thimidine and some others. This work was followed by the series of studies where the applicability of LIAD to the MS analysis of a wide range of organic samples has been demonstrated. The LIAD volatilization method was successfully coupled with Fourier transform ion cyclotron resonance mass spectrometer and alanylglycine (Reid, Tichy et al. 2001), saturated hydrocarbons (Campbell, Crawford et al. 2004), polyethylene (Campbell, Fiddler et al. 2005) and even petroleum distillates (Crawford, Campbell et al. 2005) were analyzed. The great advantages of this technique were the ability to efficiently volatilize various organics and the simplicity of its incorporation into different classes of MS instruments, such as Linear Quadrupole Ion Trap MS (Habicht, Amundson et al. 2010) and Time-of-Flight MS (Zinovev, Veryovkin et al. 2007). Various approaches for the ionization of the desorbed molecules were successfully employed, among them: electron impact and chemical ionization (Crawford, Campbell et al. 2005), single-photon ionization (SPI) (Zinovev, Veryovkin et al. 2007), as well as Elecro- Spray Ionization (ESI) (Cheng, Huang et al. 2009). Moreover, the ability of the LIAD process to non-destructively eject from solid surfaces not only single molecules but also larger intact biological particles, such as viruses (Peng, Yang et al. 2006) and 1 μm size tungsten particles (Menezes, Takayama et al. 2005) have been demonstrated.

In our opinion, the wider spread of LIAD among analytical MS applications is now limited by the lack of an adequate theoretical concept able to explain the existing observations and to predict optimal experimental conditions for future measurements. The mechanical "shake-off" model was proposed only as a qualitative explanation of observed desorption process, and as such was never used to obtain any quantitative agreement between the observable LIAD parameters and the generated acoustic waves. Moreover, to date, there was no work published in the literature, which would be devoted to systematic studies of physical parameters of the molecules desorbed by LIAD. Since we have attempted such as study, we feel it would be beneficial for the research community if we describe here briefly our own experimental methods and experimental results on LIAD.

3.3 Energy and velocity distributions of desorbed molecules

Because the dominant fraction of the desorbed flux in LIAD are neutral molecules, it is very important to select an appropriate ionization method for the molecules as well as the type of their mass analysis technique. Single-photon ionization (SPI) is well suited for characterization of this phenomenon (Pellin, Calaway et al. 2001) because of its ability to efficiently ionize the desorbing flux with minimal fragmentation. SPI occurs following absorption of a single photon whose energy exceeds the ionization potential (IP) of the molecule of interest, creating a cation. For many molecules, particularly those with aromatic rings to stabilize the cation, fragmentation from photoionization is minimized, and thus the state of the initial LIAD flux can, in principle, be revealed(Lipson and Shi 2002). Currently, the shortest wavelength of commercially available energetic lasers suitable for SPI is 157 nm (F_2 laser), which corresponds to the photon energy of 7.9 eV. This energy limits the range of species that can be ionized by SPI to atoms and molecules with IPs less than 7.9 eV. Therefore, organic dyes were chosen as analytes for this LIAD study due to their low IPs, ability to form stable cations, and high photon absorption coefficients. We selected dyes that have IPs in the range from 5 eV to 7 eV and can be easily ionized by the F_2-laser radiation.

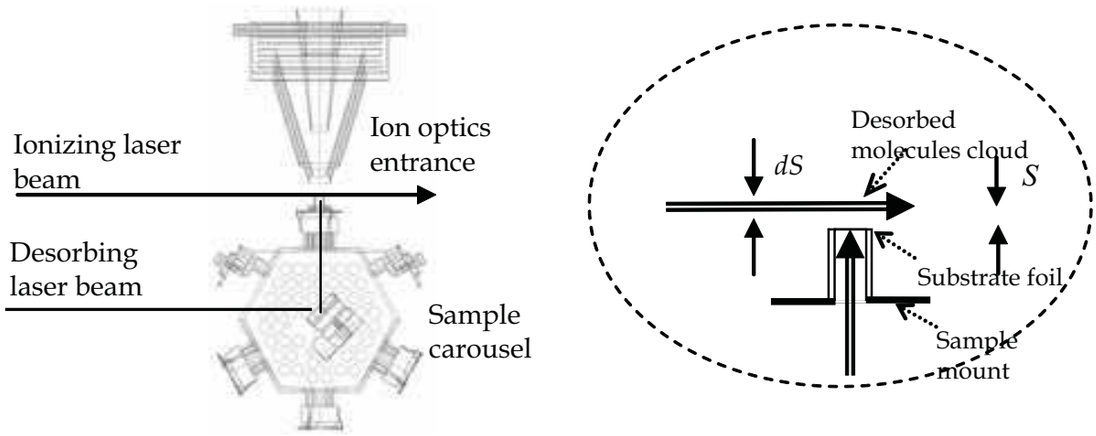

Fig. 5. Schematic drawing of target assembly and laser irradiation pathways. On the right the enlarged view of desorption/ionization scheme is displayed

A time-of-flight mass spectrometer (TOF MS) with a combined LIAD/SPI ion source was employed in our studies of the LIAD phenomenon. The experiments were conducted under ultra high vacuum conditions, with the residual gas pressure in the sample chamber less than 3×10^{-7} Pa. The schematic drawing of the target assembly in our instrument is shown in Fig. 5. The sample was mounted on one of six sample holders that were supported by a hexagonal carousel. This carousel was driven by an ultrahigh-vacuum compatible motion stage with closed-loop precision of better than 50 nm. The sample holders were secured on the carousel via three 30 mm long alumina ceramic insulators and connected (using vacuum feedthroughs) to a high-voltage pulser unit, which provided voltages necessary for the operating of TOF MS instrument. Each new sample was inserted into the UHV chamber through a vacuum loadlock. Using the motion stage, the sample was then positioned in the focal plane of the TOF MS source optics. The ion optics and operational principles of our instrument are described in more detail elsewhere (Veryovkin, Calaway et al. 2004). A

dielectric mirror with 98% reflection at 248 nm was mounted in the center of the carousel, in order to deliver the laser beam to the back side of the sample. Note that we will use the convention that the front of the sample is the side facing the ion source and TOF, while the back side is the opposite. For desorption, an excimer KrF laser with wavelength 248 nm (EX10/300 GAM Laser Inc.) was used. The output energy of the laser pulse could be varied between 0.5 - 5 mJ by adjusting the laser discharge voltage and by an additional attenuation with a set of neutral optical filters. The driving laser beam was focused on the target back surface into a spot of rectangular shape ~200×800 μm^2 by the fused silica lens with focusing distance of 500 mm. The laser pulse duration was 7 ns, producing a peak power density on the irradiated surface ranging from 50 to 500 MW/cm^2. These laser intensities are close to those used in most of LIAD experiments (Perez, Ramirez-Arizmendi et al. 2000; Campbell, Crawford et al. 2004; Campbell, Fiddler et al. 2005; Crawford, Campbell et al. 2005) taking into account that the reflection coefficient in the UV is normally less than it is at visible wavelengths. Post-ionization of the desorbed molecules was performed with an F_2 laser, with output energy of 2 mJ/pulse, and pulse duration of 10 ns. The F_2 laser beam was focused just above the front target surface, with a waist of 400×2000 μm^2, using of a combination of MgF_2 spherical and cylindrical lenses. The F_2 laser radiation power density in the focal plane was ~10 MW/cm^2, which assured the saturation of the photoionization process for the investigated molecules (as verified by a laser power study).

For comparison with LIAD, direct laser desorption (LD) mass spectra were measured for the same samples, also using the F_2 laser for post-ionization. To this end, an N_2 laser (337 nm wavelength, 100 μJ/pulse energy and 7 ns pulse duration) was focused onto the target front surface using an in-vacuum Schwarzschild optical microscope (Veryovkin, Calaway et al. 2004). The beam spot size on the surface was about 50 μm in diameter.

The delay between the driving KrF (or N_2) laser pulses and the ionizing F_2 laser could be precisely controlled and varied from 0 to 1000 μs. The desorbed molecules that move away from the surface could therefore be ionized at a precisely defined moment in time and volume in space above the target after the desorption event, with the photoions then analyzed by the TOF MS. This approach allowed us to measure mass spectra for the (postionized) desorbed neutral molecules and determine their velocity distribution. Each mass spectrum was the sum of 128 individual acquired spectra. To prevent the rise of the average foil temperature due to adsorption of laser power, the repetition rate of the laser pulses was maintained at 8 Hz.

Foils from different materials with different thicknesses were used in the experiments. The foil preparation procedure was the same as described in paragraph 2.2.3.1. Before applying the analyte to the top surface of the foil, each substrate was cleaned in methanol-acetone solution (1:1) in an ultrasonic bath (10 minutes).

Organic dyes rhodamine B, fluorescein, methylanthracene (MA), coumarin-522 (N-Methyl-4-trifluoromethylpiperidino3,2-gcoumarin), and BBQ (4,4″-Bisbutyloctyloxy-p-quaterphenyl) were used as received (Eastman Kodak). The dyes were dissolved in methanol (for MA and BBQ, mixed xylenes were also used as solvent), and then the resulting solution (about 10^{-3} M) was used for sample preparation. One μl of the analyte solution was pipetted onto the foil surface, and then the quartz cylinder-foil assembly was spun at 4500 rpm for 30 seconds to coat the analyte uniformly over the surface. During spin-coating, a significant part of the solution (90% or more) was taken off the surface and, surface concentrations of the analyte could be estimated to be less than 0.5 nM/cm^2. After the sample preparation, the foil was introduced into the instrument via the loadlock for analysis.

In good agreement with the previously published results on LIAD, we detected strong and stable desorption signals from foils with thickness of 12.5 μm (Fig. 6). Thicker foils (25 μm) produced relatively weak signals for the range of acoustic wave driven laser intensities used in our experiments. For comprehensive experiments, a Ta foil with 12.5 μm thickness was chosen as optimal, not only because high desorption signals were detected from it, but also for its good mechanical strength, high melting point, and durability under powerful laser irradiation. The TOF mass spectra of different organic dye molecules desorbed from the front of the back-irradiated Ta foil surface and ionized by the 157 nm laser radiation are shown in Fig.6. This figure shows three major features, (1) all analytes display large parent molecular ion signals, (2) all spectra display a small number of peaks, with a few or none in the mass range below 100 Da., (3) the number of fragment ion peaks is specific to each molecular analyte. In order to characterize the desorption process in terms of the corresponding molecular fragmentation, a parameter ς, can be defined as a ratio of the sum of intensities of the fragment peaks A_f to the parent molecular peak intensity A_p , $\varsigma = \sum A_f / A_p$. As will be shown below, this parameter depends on laser intensities that drive the acoustic waves. For SPI , the parameter ς characterizes not only the peculiarities of the desorption process, but it also generally depends on the photoionization cross-section of the parent molecule and specifics of its photofragmentation such as possible decay channels and their activation energies.

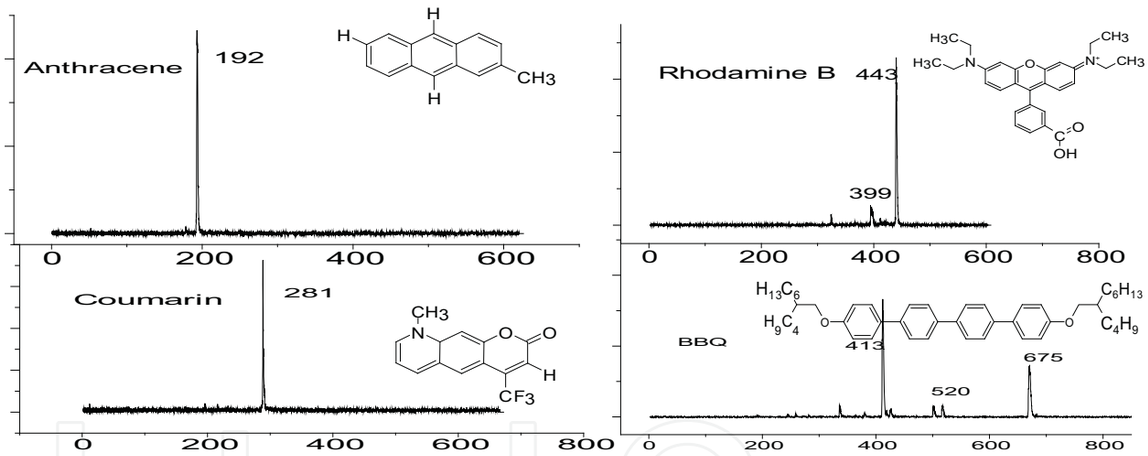

Fig. 6. Mass spectra of organic dyes in LIAD experiments

For rhodamine B, the parameter ς grew linearly with KrF laser intensity (Fig. 7), and a similar behavior was also detected for fluorescein, although values of ς were different (ς =0.8 for fluorescein at 300 MW/cm2 of KrF laser intensity). On the contrary, the same experiments conducted for BBQ, surprisingly revealed that the parameter ς decreased with increasing desorption laser power. This discrepancy in ς parameter dependency may indicate that the relationship between these two observations is not a trivial one. This raises the question of whether the desorption and fragmentation phenomena are driven by the same fundamental process. We note that fragmentation is not intrinsic to LIAD. In our experiments, we observed some indications of fragmentation for only three analytes out of five. The analysis of existing data from the literature shows that in some cases fragmentation was observed even with soft ionization of the desorbed molecules whereas in other cases fragmentation was very small or completely absent. A detailed study of

fragmentation in LIAD has not been done yet and the presented here results are the first attempt to quantify this characteristic of LIAD.

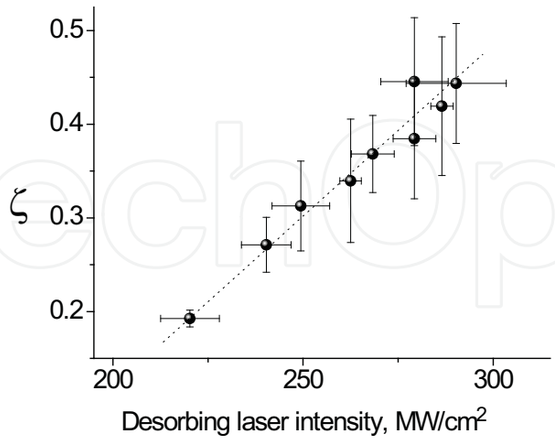

Fig. 7. Power dependence of fragmentation parameter

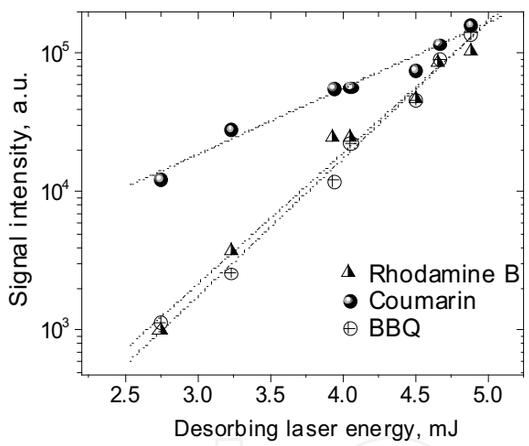

Fig. 8. Power dependence of total desorption yield for rhodamine B molecules

An important characteristic of any desorption phenomenon is its yield. This is why in order to understand the basic processes driving the phenomenon, one has to identify external parameters that have the strongest effect on the desorption yield and then measure a dependence of the yield for each parameter. In the case of LIAD, the dependence of key peak intensities in the mass spectra and the ς parameter on the driving laser intensity appears to be the most important for understanding this phenomenon. The overall desorption yield for all studied analytes strongly increased with desorption laser intensity (within our experimental range), displaying for most peaks approximately exponential dependency. Figure 8 demonstrates this dependence clearly. Plotted on a semi-logarithmic scale, these dependences appear linear, with different slopes for each analyte.

For the characterization of physical nature of the desorption processes, the knowledge of velocity distributions of desorbed neutral molecules is extremely important (Levis 1994). As

mentioned above, time-of-flight mass spectra of such molecules can be measured using the laser post ionization (LPI) technique (Spengler, Bahr et al. 1988). This experimental arrangement makes it possible to determine the distribution of the desorbed neutral molecules over their translational velocities (in the direction normal to the substrate surface) by varying the time delay between desorbing and post-ionizing laser pulses. Raw experimental data in this case are the dependencies of the observed signal on the laser delay time, called below as *signal-vs-delay* dependencies. In order to be able to directly compare LIAD and LD results, the energies of the desorbing N_2 (LD) and KrF (LIAD) lasers were adjusted such that the output molecular ion signals reached about the same intensities for the same gains of the TOF MS detector.

In good agreement with the previous experiments (Perez, Ramirez-Arizmendi et al. 2000), dramatic differences between LIAD and LD in widths of the *signal-vs-delay* dependencies and in positions of their maximums have been observed in these measurements. The most tempting explanation for this experimental finding was that the mean velocities of desorbed molecules in LIAD and LD processes were very different. Unfortunately, no actual energy or velocity distributions of desorbed molecules in LIAD process have been measured experimentally and reported in the literature to date. For the first time, this gap in knowledge can now be filled by processing our experimental data from the *signal-vs-delay* dependencies and converting them into kinetic energy distributions corresponding to our experimental conditions.

Our experiment geometry (Fig.5) is rather common, and the detailed discussion of the method as well as the appropriate conversion equations can be found elsewhere (Young, Whitten et al. 1989; Balzer, Gerlach et al. 1997). Typical values of the distance S and the thickness of ionization volume dS were set to 3 and 0.4 mm, respectively. While, as mentioned above, the value of S could be varied in our experiments between 1 mm and 5 mm, in order to achieve optimal compromise between the energy/velocity resolution and the signal-to-noise ratio, most of our data were obtained at S=3 mm. At this distance, the relative velocity resolution was $dv/v=dS/S$=0.4/3=0.13 and, correspondingly, the energy resolution was dE/E=0.18. A typical velocity distribution obtained for rhodamine B is demonstrated on Fig.10. It is apparent that the desorbed molecules in LIAD are very slow. The average velocities of rhodamine B and BBQ molecules were found to be 59±12 m/s and 47±9 m/s, respectively. For methylanthracene and coumarin522 molecules, the measured average velocities were 76±20 m/s and 70±18 m/s. It is important to recognize that these LIAD-desorbed molecules are much slower than what could be expected assuming the thermal mechanism of LIAD. In order to fit these rhodamine B data with Maxwellian distributions (dashed curve on Fig.10), physically unrealistic low temperatures of about 100 K, were required. On the other hand, the measured velocities are much higher than that of the laser-induced acoustic motion of the foil surface in normal direction, which, measured in the same experimental arrangement, did not exceed 1 m/s. This observation caused serious doubts on the validity of the "shake-off" mechanism considered by many as the most likely cause of LIAD. The measurements of velocity distribution of species desorbed in LD geometry were used for direct comparison with LIAD, and as the proof of validity of our experimental procedure. A smaller insert plot on Fig.10 demonstrates the velocity distribution of desorbed rhodamine B main fragment (399 amu) obtained in the LD irradiation scheme. The mechanisms of the velocity distribution formation in the LD process are well-known and discussed in many reviews (Levis 1994). According to a commonly used procedure described in (Natzle, Padowitz et al. 1988), this distribution can be fit by a

two-temperature bi-modal velocity distribution: dashed lines in the insert plot represent spectral components with different temperatures, and the solid line corresponds to their sum. Being in a good agreement with general LD regularities, these results also confirm the validity of the experimental procedure used for both LD and LIAD.

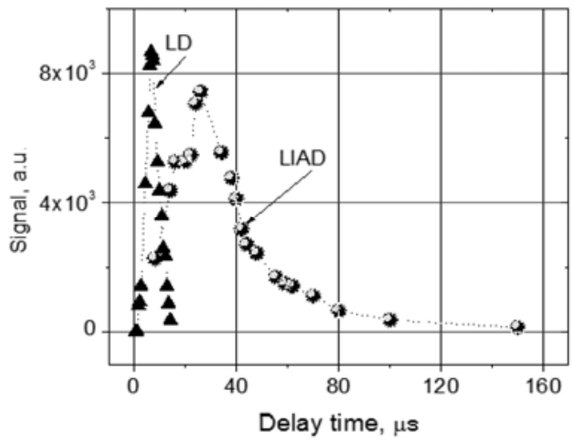

Fig. 9. The comparison of *signal-vs-delay* for LIAD and LD desorbed rhodamine B molecules

Velocity distributions were measured also at different fluences of the driving KrF laser. On Fig. 10, two distributions corresponding to laser fluences of 2.3 J/cm² and 3.4 J/cm² are plotted. Within the limits of accuracy of our measurements, no change of average velocity has been detected, which suggests that both thermal and "shake-off" models are not applicable for the explanation of LIAD process.

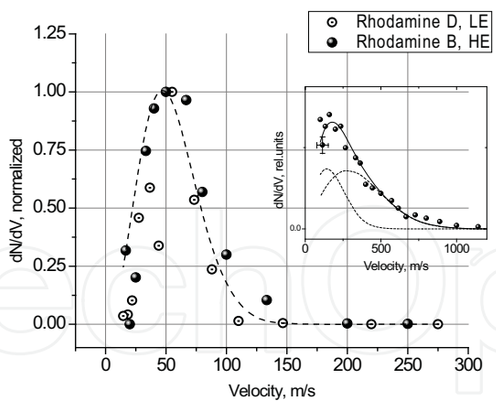

Fig. 10. Velocity distribution for rhodamine B molecules at different LIAD desorption laser intensities. On insert there is the same distribution for LD regime

In order to calculate the mean energies of desorbed molecules, we used the described above approach and took into account that the Jacobian of this variable transformation was given by S^2/t^3 (Balzer, Gerlach et al. 1997). The mean energies of molecules in LIAD experiments (as well as their mean velocities) showed no apparent trend with the increase of desorbing laser fluences keeping the average value at about 9 meV for rhodamine B, 9.5 meV for BBQ, 6.5meV for coumarine 522 and 7.5meV for methylanthracene. Typical energy distributions

measured for these molecules are shown on Fig.11. Dashed line represents Maxwell distribution for rhodamine B corresponding to the 80 K temperature. This temperature was chosen to obtain the best fit at the distributions maximums. At the same time, high energy tails of the experimental energy distributions strongly deviate from the exponential law, which is apparent with the double logarithmic scale in Fig.11, and reveal behavior close to the power dependence.

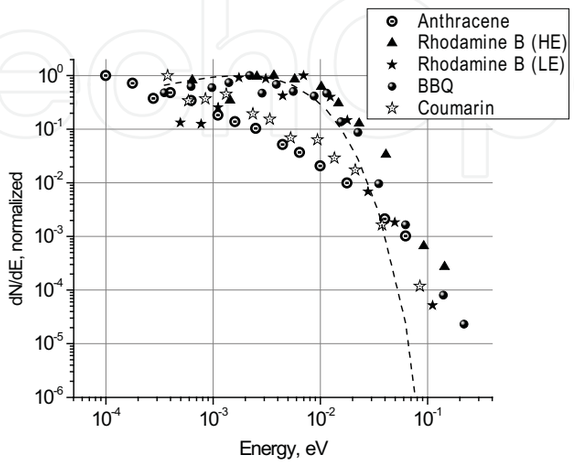

Fig. 11. Energy distribution of different organic dyes molecules. Dashed line represents equilibrium Boltzmann distribution at T=100 K

4. Is desorption process in LIAD really driven by acoustic waves?

4.1 "Shake-off "mechanism versus thermal origin of molecular desorption

The "shake-off" mechanism of molecular desorption in LIAD for a long time was considered as the only sensible explanation of the observed phenomenon. However, as was shown above, it contradicts both with general physical considerations and with the experimentally measured parameters of acoustic vibrations of the surface as well as with the observed energy and velocity spectra of desorbed molecules.

An important consequence of the backside irradiation is the heating of the front side. Considering this effect, we should keep in mind that this heating process in LIAD is distinctly different from the case of direct front-side laser irradiation (LD). In the latter case, due to the small value of skin depth in metals, the rate of the temperature rise is extremely high. In case of backside irradiation of the foils, the front surface temperature is governed by the heat conduction through the metal foil, which makes the heating rate much slower than that for the front side irradiation geometry. For one-dimensional heat conduction problem, the specific time of the temperature rise is defined by the heat propagation time $\tau = l^2 / \alpha$, where a is the thermal diffusivity of the metal and l is the foil thickness. For the foil thicknesses typical for LIAD (~10 μm) and the thermal diffusivity of the most metals $a \approx 0.2 - 0.7$ cm^2·s^{-1}, τ has the values in the range of a few μs. Our numerical calculations using the heat conduction equation showed that for Ta foil with the thickness of 12.5 μm and the driving laser fluence 3.5 J/cm^2 (corresponding under conditions of our experiments to the peak laser intensity of about 500 MW/cm^2), the front surface temperature rise is 375 K, which reaches its maximum 1.75 μs after the laser desorbing pulse ceases. If experiments

start with room temperatures, the peak foil surface temperatures then can reach 668÷673 K. Because the melting point of rhodamine B is just 438 K, the thermal origin of the LIAD process can, in fact, come into the focus of our consideration. However, other experimental results obtained in this work, make this mechanism very unlikely. These results are:

1. rather small fragmentation of molecules in LIAD, compared to that for LD;
2. distinct differences in velocity and energy distributions between LIAD and LD;
3. slow velocities and low kinetic energies of desorbed molecules compared to those required by the thermal mechanism;
4. the apparent independence of mean energies of the desorbed molecules in LIAD on the driving laser fluence (also observed by by Kenttamaa et al. in their recent work (Shea, Petzold et al. 2007).

Moreover, the mechanical "shake-off" mechanism is also in contradiction with the observation (4), because the amplitudes and velocities of laser generated acoustic waves should increase with the driving laser fluencies. Thus we can conclude that both mechanisms of the direct energy transfer (acoustic waves and heat conduction) cannot serve as the primary explanation of the LIAD phenomenon, and apparently more complicated processes are involved here.

4.2 Stress and strain of the foil surface due to the laser irradiation

It is a well-known fact that a film deposition on a substrate surface results in many cases in the residual mechanical stress (due to the lattice parameters mismatch between the film and the substrate) and thus in some excessive potential energy stored in the film. This stress can be produced by two ways: one is the growth stress and the other is the induced (or extrinsic) stress (Freund and Suresh 2003). An external impact, such as acoustic or thermal wave generated by the laser irradiation of the substrate, should initiate the reconstruction of the film, which can result in releasing this excess energy or, possibly, generating an additional extrinsic stress. In both cases, it can cause formation of cracks in the film so that intermolecular bonds at the edges of the cracks can break. As a result of this crack formation process, excited electronic states can form at the crack edges and induce desorption of the molecules.

Despite a great variety of mechanisms of stress formation and evolution do exist, a quantitative description of this process is possible only in limited cases even for simple adsorbent-adsorbate systems. Accurate modeling of the film behavior requires precise knowledge of the thermal and mechanical properties of the film material and their interaction with substrate surface. For most organic materials, such data are unavailable, and thus only limited estimates may be done, based on the little amount of data published in the literature (Bondi 1968). Moreover, the deposited films of organic materials tend to consist of a mixture of micro-crystals with different crystallographic orientation and, therefore, there are many grain boundaries, defects, dislocations in such films that could significantly change their local mechanical properties.

A simplified numerical estimate of the stress energy, related to the thermal mismatch of the substrate foil and the analyte film on its top could be done, as follows. An equi-biaxial stress resulting from acoustic vibration of the back-irradiated metal foil may be estimated using the following expression (Boley and Weiner 1960; Freund and Suresh 2003)

$$\sigma_m = \frac{E \cdot h_f}{R \cdot (1-\nu)} \tag{16}$$

where E is the Young's modulus, v is the Poisson ratio, h_f is the thickness of organic film and R is the radius of curvature of the foil surface. From the other side, the stress, resulting from thermal mismatch has the following value (Boley and Weiner 1960)

$$\sigma_t = (\alpha_s - \alpha_f) \cdot \Delta T \cdot E / (1 - \nu), \tag{17}$$

where a_s and a_f are thermal expansion coefficients of the substrate and the film respectively, ΔT is the temperature increase. There is not much information in the literature on thermo-mechanical parameters for molecular crystals but based on existing data for anthracene (Bondi 1968) we can estimate the order of the generated stress values. Under the assumption that $\boldsymbol{a_f}$ =2.8 ·10^{-4} K^{-1} , $\boldsymbol{a_s}$ = 6.3 ·10^{-6} K^{-1}, E= 13 GPa, v≈0.25, and ΔT=100 K, we can obtain σ_t=485 MPa. At the same time, the stress associated with acoustic vibrations is much lower: σ_m≈1.7 kPa (taking into account that maximal value of R is approximately 1 m, and the film thickness never exceeded 10^{-7} m,). This is a negligible value, in comparison with σ_t , which means that the thermal mismatch stress is the principal reason for cracks formation. The estimate of internal energy, stored in thermally strained organic films can be done with using of following expression (Boley and Weiner 1960)

$$G = \frac{E \cdot (1+\nu)^2}{2 \cdot (1-\nu^2)} \cdot (\alpha_s - \alpha_f)^2 \cdot \Delta T^2 \cdot 2 \cdot \pi \cdot r_0 \cdot h_f \tag{18}$$

The average energy per analyte molecule can easily be calculated

$$g_a = \frac{E \cdot (1+\nu)^2}{2 \cdot (1-\nu^2) \cdot \rho} \cdot \frac{(\alpha_s - \alpha_f)^2 \cdot \Delta T^2 \cdot M}{N_A} \tag{19}$$

Here M is the molar mass, ρ is the specific gravity and N_A is the Avogadro number. It is interesting to note that g_a does not depend on the analyte island size but strongly depends on the thermal and mechanical parameters. Again with the use of existing data for anthracene we can estimate the value of g_a, and for ΔT=100 K we will get g_a=0.025 eV . This is not enough to break intermolecular bonds but when thermally induced stress exceeds a critical value, the film can start to fracture and the stored energy is released in a small volume in the vicinity of the stress cracks. Due to the strong spatial nonuniformity of thermo-mechanical properties of molecular crystals (Bondi 1968) the physical mechanisms involved in this process are very complicated in nature; therefore we can give only a qualitative picture of this phenomenon. Presumably, the cracks are formed along grain boundaries, defects and interfaces. The increase of the desorption laser intensity that causes a rise in ΔT and, in accordance with Eq. 18, an increase in energy G, results in the formation of additional cracks. Some part of this excess energy can be then converted into the increased free surface energy, other part – into electronic excitations, but because these processes are obviously non-adiabatic, the crack formation most likely will be accompanied by breaking intermolecular bonds and forming new desorption sites.

4.3 Proposed mechanisms of the molecules desorption

The desorption process itself appears to be the most obscure part of the LIAD phenomenon. The formation of the electronically excited states on the surface due their mechanical fracture is considered to be the main physical nature of triboemission (Nakayama, Suzuki et al. 1992), also known as “Kramer effect” (Oster, Yaskolko et al. 1999; Oster, Yaskolko et al.

2001). The essence of this effect is the emission of charged particles and photons initiated by surface distortion (in particular by mechanical deformation, scratching, bending, etc.) and do not connected with thermal excitation. The luminescence of thin metal discs, irradiated from back side by the laser pulses (Abramova, Shcherbakov et al. 1999; Abramova, Rusakov et al. 2000) can also serve as evidence of formation of excited electronic states by the laser-driven stress in thin foils.

The mechanism of molecular desorption due to such laser-generated stress has been proposed earlier by Vertes (Vertes and Levine 1990; Vertes 1991) for MALDI, and was based on the thermal stress generation in the layer of organic film deposited on solid substrates. One should notice, however, a clear differences in the physical conditions between these sample volatilization methods. For MALDI, the absorption of the laser pulse energy occurs in an optically and thermally dense film, which experiences thermal stress due to its non-uniform and fast heating. In the case of LIAD, the laser radiation is absorbed by the back side of the metal foil substrate, opposite from where the sample was deposited. The amount of energy transmitted through the metal foil to the analyte layer on the front site should be so strongly attenuated, compared to the direct (front side) irradiation, that it cannot directly be sufficient for desorbing molecules with velocities observed in our experiments. On the other hand, a typical average thickness of the analyte film in LIAD can be estimated to be on the order of several molecular layers. Because of this, the specific density of energy stored in each analyte island due to intrinsic stress can be high, and during laser irradiation of the back side of the foil, the laser irradiation can simply trigger the release of this energy and to induce molecular desorption event.

The other experimental fact that could help in the interpretation of LIAD phenomenon is the similarity of the energy and velocity spectra of desorbed neutral molecules in case of LIAD and Electron Stimulated Desorption (ESD) (Young, Whitten et al. 1989). The primary mechanism of ESD is supposed to be the formation of the repulsive states in the surface due to electron excitation.

Thus we could hypothesize that in case of LIAD, due to complete opaqueness of metal foil for laser radiation, the only channel for energy transfer is the formation of acoustic and thermal field by laser pulse impact. As shown above, the result can be the mechanical distortion of the analyte film followed by film cracking and delamination and the consequent formation of excited and repulsive states electronic for analyte molecules.

This will increase the number of desorption sites and finally the total number of desorbed molecules as observed in the nonlinear laser intensity dependence. But because the formation of the any individual cracks is defined only by the intermolecular bonding forces in the vicinity of the crack, the translational kinetic energy of desorbed molecules should still remain independent of driving laser intensity, also matching our observations and other recent LIAD publications.

5. Conclusion

Traditionally, the name LIAD combine all desorption phenomena taking place when an opaque target is irradiated from the back side, ignoring differences in experimental conditions. In our opinion, it is not correct. As it was demonstrated in this work, under some experimental conditions (most commonly used in many present studies), the physical origin of the observed desorption phenomenon is not (and could not be) connected with the acoustic waves generated in the foil and most likely is defined by the film stress and

cracking due to thermal and mechanical mismatch of the analyte and substrate. Therefore, ironically, the acronym LIAD in this case does not correctly reflect the physical nature of the process.

From the other hand, we cannot exclude that some strong change of the experimental conditions can also change the relationship between various physically possible mechanisms of molecular desorption, similarly to the case of direct laser desorption, when the thermal mechanism dominates under wide range of conditions and makes other possible mechanisms undetectable. One can expect, for example, that strong increase of laser power density (10 GW/cm^2 and above) will cause the corresponding increase of the foil temperature and formation of hot and dense plasma plume near its surface facing the laser. In some such cases and strongly depending on the foil material properties, the material motion could evolve from elastic into plastic regime of deformation. The acoustic wave relation could not then apply, and the velocity of the surface linear motion may strongly increase. "Large and heavy" objects weakly bound to the substrate surface may be then kinematically removed from it ("shaken-off"). This could indeed serve as an explanation of observations from recent experiments where the desorption of intact viruses and biological cells were reported (Peng, Yang et al. 2006). However, this regime cannot be connected with generation of the acoustic waves but most likely corresponds to a physically different mode of shock-wave generation (Menikoff 2007). One cannot exclude that under some experimental LIAD conditions only these shock-wave induced phenomena can be responsible for molecular desorption, particularly in the experiments where emission of ions was detected. In one of such pioneering experiments (Golovlev, Allman et al. 1997), where the laser generated pressure pulse was apparently much stronger than that in our work, because of confined ablation conditions (Fabbro, Fournier et al. 1990), the emission of both electrons and ions was observed. This may have been connected with significant surface disruption at the microscale generated by shock waves.

From another standpoint, the backside irradiation of very thin films (about two or three hundred nanometers), which also could be called LIAD, has demonstrated domination of the thermal mechanism in the desorption process (Ehring, Costa et al. 1996). It is clear that the thermal equilibrium between front and back sides in such thin films can establish within the time interval of tens of nanoseconds, and the absolute temperature difference between front and back sides is negligibly small. Thus, at some laser power densities, the front side temperature could reach the melting temperature of the metal that would be enough to cause an efficient thermal desorption of the most organic molecules.

To conclude, the variety of desorption and emission phenomena observed on the front side of thin metal foils whose back sides are subjected to pulsed laser irradiation, combined under the general name of LIAD, could, in fact, have a number of different physical origins depending on specific experimental conditions. According to our observations conducted at moderate laser power densities (0.1 - 1 GW/cm^2) and foils thicknesses of about 5 – 20 μm, that appear to be the most commonly used conditions in LIAD experiments, the predominant desorption mechanism is connected with the reorganization of the deposited analyte film and the consequent breaking of molecular bonds on the edges of these cracks.

6. Acknowledgment

This work is supported by the U.S. Department of Energy, BES-Materials Sciences, under Contract DE-AC02-06CH11357, by UChicago Argonne, LLC.

7. References

Abramova, K. B., A. I. Rusakov, et al. (2000). Photon emission from metals under fast nondestructive loading. *J. Appl. Phys.* 87(6): 3132-3136.

Abramova, K. B., I. P. Shcherbakov, et al. (1999). Emission processes accompanying deformation and fracture of metals. *Phys.Solid State* 41(5): 761-762.

Adamson, A. W. and A. P. Gast (1997). Physical Chemistry of Surface. New York, John Wiley &Sons, Inc.

Balzer, F., R. Gerlach, et al. (1997). Photodesorption of Na atoms from rough Na surface. *J. Chem. Phys.* 106(19): 7995-8012.

Boley, B. A. and J. H. Weiner (1960). Theory of thermal stresses. New York,, Wiley.

Bondi, A. (1968). Physical properties of molecular crystals, liquids and gases. New York, London, Sydney, Hohn Wiley & Sons.

Campbell, J. L., K. E. Crawford, et al. (2004). Analysis of saturated hydrocarbons by using chemical ionization combined with laser-induced acoustic desorption/Fourier transform ion cyclotron resonance mass spectrometry. *Analytical Chemistry* 76(4): 959-963.

Campbell, J. L., M. N. Fiddler, et al. (2005). Analysis of polyethylene by using cyclopentadienyl cobalt chemical ionization combined with laser-induced acoustic desorption/Fourier transform ion cyclotron resonance mass spectrometry. *Analytical Chemistry* 77(13): 4020-4026.

Cheng, S. C., M. Z. Huang, et al. (2009). Thin-Layer Chromatography/Laser-Induced Acoustic Desorption/Electrospray Ionization Mass Spectrometry. *Analytical Chemistry* 81(22): 9274-9281.

Cole, R. B. (2010). Electrospray and MALDI mass spectrometry: fundamentals, instrumentation, practicalities, and biological applications. Hoboken, N.J., Wiley.

Crawford, K. E., J. L. Campbell, et al. (2005). Laser-induced acoustic desorption/Fourier transform ion cyclotron resonance mass spectrometry for petroleum distillate analysis. *Anal. Chem.* 77(24): 7916-7923.

Crawford, K. E., J. L. Campbell, et al. (2005). Laser-induced acoustic desorption/Fourier transform ion cyclotron resonance mass spectrometry for petroleum distillate analysis. *Analytical Chemistry* 77(24): 7916-7923.

Dass, C. (2007). Fundamentals of contemporary mass spectrometry. Hoboken, N.J., Wiley-Interscience.

Duncan, M. W., H. Roder, et al. (2011). Quantitative matrix-assisted laser desorption/ionization mass spectrometry. *Briefings in Functional Genomics* 7(5): 355-370.

Ehring, H., C. Costa, et al. (1996). Photochemical versus thermal mechanisms in matrix-assisted laser desorption/ionization probed by back side desorption. *Rapid Communications in Mass Spectrometry* 10(7): 821-824.

Fabbro, R., J. Fournier, et al. (1990). Physical Study of Laser-Produced Plasma in Confined Geometry. *Journal of Applied Physics* 68(2): 775-784.

Freund, L. B. and S. Suresh (2003). Thin Film Materials. Stress, Defect Formation and Surface Evolution. Cambridge, Cambridge University Press.

Golovlev, V. V., S. L. Allman, et al. (1997). Laser-induced acoustic desorption of electrons and ions. *Applied Physics Letters* 71(6): 852-854.

Gospodyn, J. P., A. Sardarli, et al. (2002). Ablative generation of surface acoustic waves in aluminum using ultraviolet laser pulses. *Journal of Applied Physics* 92(1): 564-571.

Habicht, S. C., L. M. Amundson, et al. (2010). Laser-Induced Acoustic Desorption Coupled with a Linear Quadrupole Ion Trap Mass Spectrometer. *Analytical Chemistry* 82(2): 608-614.

Honig, R. E. and J. R. Woolston (1963). Laser-induced emission of electrons, ions and neutral atoms from solid surfaces. *Applied Physics Letters* 2(7): 138-139.

Hutchins, D. A. (1985). Mechanisms of Pulsed photoacoustic generation. *Can. J. Phys.* 64: 1247-1263.

Karas, M., D. Bachmann, et al. (1985). Influence of the Wavelength in High-Irradiance Ultraviolet-Laser Desorption Mass-Spectrometry of Organic-Molecules. *Analytical Chemistry* 57(14): 2935-2939.

Krehl, P., F. Schwirzke, et al. (1975). Correlation of Stress-Wave Profiles and Dynamics of Plasma Produced by Laser Irradiation of Plane Solid Targets. *Journal of Applied Physics* 46(10): 4400-4406.

Landau, L. D. and E. M. Lifshits (1987). Fluid mechanics. New York, Pergamon.

Levis, R. J. (1994)."Laser-Desorption and Ejection of Biomolecules from the Condensed-Phase into the Gas-Phase. *Annu. Rev. Phys. Chem.* 45: 483-518.

Lindner, B. and U. Seydel (1985). Laser Desorption Mass-Spectrometry of Nonvolatiles under Shock-Wave Conditions. *Analytical Chemistry* 57(4): 895-899.

Lipson, R. H. and Y. J. Shi (2002). Ultraviolet Spectroscopy and UV lasers. New York-Basel, Marcel Deccer, Inc.,.

Lubman, D. M. (1990). Lasers and mass spectrometry. New York, Oxford University Press.

McLachlan, N. W. (1951). Theory of vibrations. New York, Dover Publications.

Menezes, V., K. Takayama, et al. (2005). Laser-ablation-assisted microparticle acceleration for drug delivery. *Applied Physics Letters* 87(16): -.

Menikoff, R. (2007). Empirical Equations of State for Solids. *Shock Wave Science and Technology Reference Library*. Y. Horie. Berlin, Springer. 2: v. <1-3>.

Miller, J. C. and R. F. Haglund (1998). Laser ablation and desorption. San Diego, Academic Press.

Mora, P. (1982). Theoretical-Model of Absorption of Laser-Light by a Plasma. *Physics of Fluids* 25(6): 1051-1056.

Murray, T. W. and J. W. Wagner (1999). Laser generation of acoustic waves in the ablative regime. *Journal of Applied Physics* 85(4): 2031-2040.

Nakayama, K., N. Suzuki, et al. (1992). Triboemission of Charged-Particles and Photons from Solid-Surfaces during Frictional Damage. *J. Phys. D: Appl. Phys.* 25(2): 303-308.

Natzle, W. C., D. Padowitz, et al. (1988). Ultraviolet-Laser Photodesorption of No from Condensed Films - Translational and Internal Energy-Distributions. *Journal of Chemical Physics* 88(12): 7975-7994.

Oster, L., V. Yaskolko, et al. (1999). Classification of exoelectron emission mechanisms. *Physica Status Solidi a-Applied Research* 174(2): 431-439.

Oster, L., V. Yaskolko, et al. (2001). The experimental criteria for distinguishing different types of exoelectron emission mechanisms. *Physica Status Solidi a-Applied Research* 187(2): 481-485.

Pellin, M. J., W. F. Calaway, et al. (2001). Laser Post Ionization for Quantative Elemental Analysis. *ToF-SIMS: Surface Analysis by Mass Spectrometry*. J. Vickerman and D. Briggs, Surface Spectra Ltd. and IM Publications 375.

Peng, W. P., Y. C. Yang, et al. (2006). Laser-induced acoustic desorption mass spectrometry of single bioparticles. *Angew. Chem., Int. Ed.* 45(9): 1423-1426.

Perez, J., L. E. Ramirez-Arizmendi, et al. (2000). Laser-induced acoustic desorption/chemical ionization in Fourier-transform ion cyclotron resonance mass spectrometry. *Int. J. Mass Spectrom.* 198(3): 173-188.

Phipps, C. R., T. P. Turner, et al. (1988). Impulse coupling to targets in vacuum by KrF, HF and CO_2 single-pulse lasers. *Journal of Applied Physics* 64(3): 1083-1096.

Pollard, H. F. (1977). Sound waves in solids. London, Pion.

Prokhorov, A. M., V. I. Konov, et al. (1990). Laser Heating of Metals. Bristol, Philadelphia, New York, Adam Higler.

Reid, G. E., S. E. Tichy, et al. (2001). N-terminal derivatization and fragmentation of neutral peptides via ion-molecule reactions with acylium ions: Toward gas-phase Edman degradation? *Journal of the American Chemical Society* 123(6): 1184-1192.

Royer, D. and E. Dieulesaint (2000). Elastic waves in solids. Berlin ; New York, Springer.

Schiller, J., R. Suss, et al. (2007). Maldi-Tof Ms in Lipidomics. *Frontiers in Bioscience* 12: 2568-2579.

Scruby, C. B. (1987). An introduction to acoustic emission. *Journal of Physics E (Scientific Instruments)* 20(8): 946-953.

Scruby, C. B. and H. N. G. Wadley (1978). Calibrated Capacitance Transducer for Detection of Acoustic-Emission. *Journal of Physics D-Applied Physics* 11(11): 1487-1494.

Shea, R. C., C. J. Petzold, et al. (2007). Experimental investigations of the internal energy of molecules evaporated via laser-induced acoustic desorption into a Fourier transform ion cyclotron resonance mass spectrometer. *Analytical Chemistry* 79(5): 1825-1832.

Smith, S. T. (2000). Flexures: elements of elastic mechanisms. Amsterdam, Gordon & Breach.

Song, K. H. and X. Xu (1997). Mechanisms of absorption in pulsed excimer laser-induced plasma. *Applied Physics a-Materials Science & Processing* 65(4-5): 477-485.

Spengler, B., U. Bahr, et al. (1988). Postionization of Laser-Desorbed Organic and Inorganic-Compounds in a Time of Flight Mass-Spectrometer. *Anal. Instrum.* 17(1-2): 173-193.

Srinivasan, R. and B. Braren (1989). Ultraviolet-Laser Ablation of Organic Polymers. *Chemical Reviews* 89(6): 1303-1316.

Vertes, A. (1991). Laser Desorption of Large Molecules: Mechanisms and Models. *Methods and Mechanisms for Producing Ions from Large Moleculres*. K. G. Standing and W. Ens. New York, Plenum Press.

Vertes, A. and R. D. Levine (1990). Sublimation Versus Fragmentation in Matrix-Assisted Laser Desorption. *Chem. Phys. Lett.* 171(4): 284-290.

Veryovkin, I. V., W. F. Calaway, et al. (2004). A new time of flight instrument for quantative surface analysis. *Nucl. Instrum. Methods Phys. Res., Sect. B* 219-220: 473.

White, R. M. (1963). Generation of elastic waves by transient surface heating *Journal of Applied Physics* 34(12): 3559-&.

Xu, B. Q., J. Feng, et al. (2008). Laser-generated thermoelastic acoustic sources and Lamb waves in anisotropic plates. *Applied Physics a-Materials Science & Processing* 91(1): 173-179.

Young, C. E., J. E. Whitten, et al. (1989). Electron-Stimulated Desorption of Neutrals from 6063 Aluminum - Velocity Distributions Detected by 193 Nm Non-Resonant Laser Ionization. *Surface and Interface Analysis* 14(10): 647-655.

Zinovev, A. V., I. V. Veryovkin, et al. (2007). Laser-driven acoustic desorption of organic molecules from back-irradiated solid foils. *Analytical Chemistry* 79(21): 8232-8241.

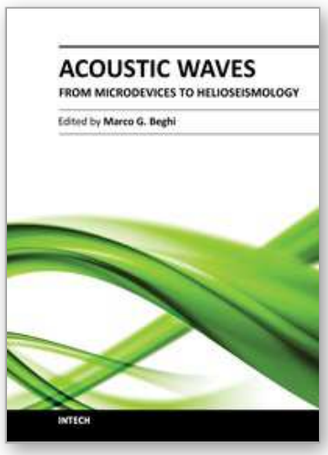

Acoustic Waves - From Microdevices to Helioseismology

Edited by Prof. Marco G. Beghi

ISBN 978-953-307-572-3
Hard cover, 652 pages
Publisher InTech
Published online 14, November, 2011
Published in print edition November, 2011

The concept of acoustic wave is a pervasive one, which emerges in any type of medium, from solids to plasmas, at length and time scales ranging from sub-micrometric layers in microdevices to seismic waves in the Sun's interior. This book presents several aspects of the active research ongoing in this field. Theoretical efforts are leading to a deeper understanding of phenomena, also in complicated environments like the solar surface boundary. Acoustic waves are a flexible probe to investigate the properties of very different systems, from thin inorganic layers to ripening cheese to biological systems. Acoustic waves are also a tool to manipulate matter, from the delicate evaporation of biomolecules to be analysed, to the phase transitions induced by intense shock waves. And a whole class of widespread microdevices, including filters and sensors, is based on the behaviour of acoustic waves propagating in thin layers. The search for better performances is driving to new materials for these devices, and to more refined tools for their analysis.

InTech Europe
University Campus STeP Ri
Slavka Krautzeka 83/A
51000 Rijeka, Croatia
Phone: +385 (51) 770 447
Fax: +385 (51) 686 166
www.intechopen.com

InTech China
Unit 405, Office Block, Hotel Equatorial Shanghai
No.65, Yan An Road (West), Shanghai, 200040, China
中国上海市延安西路65号上海国际贵都大饭店办公楼405单元
Phone: +86-21-62489820
Fax: +86-21-62489821

IntechOpen